Title: Structure-based analysis of a natural GOT1-inhibitor Aspulvinone H arrests pancreatic ductal adenocarcinoma cells growth

Running title: GOT1-inhibitor AH arrests PDAC cells growth

Shan Yan, [1] Wei Song, [2] Qianqian Xu, [1] Changxing Qi, [1*] Weiguang Sun, [1*]

Yonghui Zhang [1*]

[1] *Hubei Key Laboratory of Natural Medicinal Chemistry and Resource Evaluation, School of Pharmacy, Tongji Medical College, Huazhong University of Science and Technology, Wuhan 430030, People's Republic of China*

[2] *College of pharmaceutical science, Zhejiang Chinese Medical University, Hangzhou 310053, Zhejiang, China*

[*] Correspondence: zhangyh@mails.tjmu.edu.cn (Y. Zhang); weiguang_s@hust.edu.cn (W. Sun); qichangxing@hust.edu.cn (C. Qi)

Abstract

Pancreatic ductal adenocarcinoma (PDAC) cells are Gln-metabolism dependence, which can preferentially utilize glutamic oxaloacetate transaminase 1 (GOT1) to maintain the redox homeostasis of cancer cells. Therefore, small molecule inhibitors targeting GOT1 can be used as a new strategy for developing cancer therapies. Here, we identified a cyclobutyrolactone lignan, Aspulvinone H (AH), showing significant GOT1 inhibitory activity *in vitro*. The complex crystal structure of GOT1-AH elucidated the molecular mechanism, which AH and the cofactor pyrido-aldehyde 5-phosphate (PLP) competitively bound to the active sites of GOT1. Structure-activity relationship (SAR) analysis exhibited that the π-π stacking and isopentenyl side chain of aspulvinone were related to the inhibition of GOT1 activity. Further biological study indicated that AH could suppress glutamine metabolism, which made PDAC cells sensitive to oxidative stress and inhibited cell proliferation. Besides, AH exhibited potent *in vivo* antitumor activity in the SW1990 cell-induced xenograft model. These findings suggest that AH could be considered as a promising lead molecule for the development of PDAC anticancer agents.

Keywords: Natural products, GOT1 enzyme, X-ray crystallography, Pancreatic ductal adenocarcinoma cells, Glutamine metabolism

Introduction

Pancreatic ductal adenocarcinoma (PDAC), a highly aggressive malignancy, is estimated to become the second leading cause of cancer-related deaths by 2030, which the 5-year survival rates have constantly remained below 10% in the past decades.[1] Altering metabolism is a key indicator for cancer cells to meet their biosynthesis requirements.[2,3] Recently, it has been demonstrated that the demand for glutamine (Gln) in PDAC cells is excessive, and it promotes proliferation and tumor growth through a non-canonical Gln metabolic pathway regulated by KRAS.[4-6] In detail, the Gln derived aspartate (Asp) is transported to the cytoplasm, where glutamic-oxaloacetic transaminase 1 (GOT1) catalyzes the transformation of α-KG and Asp to Glu and oxaloacetate (OAA). Subsequently, continuous catalytic reactions of malate dehydrogenase 1 (MDH1) and malic enzyme 1 (ME1) convert OAA to Pyruvate and yield NADPH (**Fig 1A**).[7,8] PDAC cells rely on these responses to increase the NADPH/$NADP^+$ ratio to maintain the intracellular redox state.[9,10] As an essential enzyme in this pathway, the inhibition of GOT1 is profoundly growth inhibitory in PDAC cells but well tolerated by normal cells.[11] GOT1 metabolic pathways have also been shown to play a role in other malignant tumor cells including small cell lung cancer, breast adenocarcinoma and glioblastoma multiforme.[12,13] Hence, GOT1-inhibitors will be a promising tool for studying the targeting metabolism of PDAC and other Gln-dependent cancers.

From 1981 to 2019, over 60% of the small molecule anticancer drugs were directly or indirectly related to natural products (NPs).[14] Most NPs require structural

modifications to reduce the complexity or toxicity, increase activity or improve pharmacokinetics.[15, 16] With the advent of protein engineering, structure-based drug design (SBDD) strategies are more widely used and becoming increasingly powerful, which greatly accelerates the process of drug development.[17,18] Although the crystal structure of GOT1 was known, the complex structure of GOT1 and inhibitor has not been obtained.[19] Therefore, starting from NPs with higher activity, combining structural biology, chemical synthesis and pharmacological evaluation is an important way to develop innovative drugs.[20]

Aspulvinone, a class of highly functional cyclobutyrolactone lignans, are known as luciferase inhibitors.[21] In the previous study, we identified that Aspulvinone O (AO) as a potent inhibitor of GOT1, which could suppress PADC cells growth by interfering glutamine metabolism.[10] Notably, aspulvinone may be a novel anti-tumor agent which needs further exploration and development. To date, there are few studies on the pharmacological activities of aspulvinone.

Accordingly, we screened a series of cyclobutyrolactone lignans from the in-house NPs library and found that Aspulvinone H (AH) with significant inhibition of GOT1 activity. High-resolution crystal structure was obtained for the complex and revealed that AH as a PLP-competitor binding in the active site of GOT1. Structure-activity relationship (SAR) analysis showed that the conjugated structure and isopentenyl side chain of aspulvinone were related to the inhibition of GOT1 activity. Simultaneously, we found that AH could inhibit the growth of PDAC cells both *in vivo* and *in vitro*, and induce the apoptosis of cancer cells through inhibiting Gln metabolism. As a selective

GOT1 inhibitor, the complex crystal structure of GOT1-AH and the biological activity evaluation of AH will shed new light on the design and development of agents in the PDAC treatment.

Materials and Methods

Materials

General reagents and chemicals were purchased from Sigma Aldrich (St. Louis, USA). Kits were purchased from commercial sources. AH and other lignans were obtained from our laboratory (95% or higher purity).

Molecular cloning, expression and purification

The gene of got1 was C-terminal His_6-tagged and cloned into pET-26b vector (Invitrogen, USA). GOT1 were overexpressed in Escherichia coli BL21 (DE3) cells at 30°C for 6 h. His_6-tagged fusion protein was initially pulled down using Ni-NTA columns and then further purified by anion exchange chromatography with Resource Q (GE Healthcare, USA). Peak fractions containing GOT1 were concentrated firstly using 10-kDa cut-off centrifuge tubes (Millipore, USA) and subsequently using Superdex 200 Increase 10/300 GL Gel-Filtration Columns (GE Healthcare, USA). Finally, protein samples were dialyzed against a buffer containing 20 mM Hepes (pH 7.5), 200 mM NaCl.

Enzyme inhibition assays

The activity assay was performed in 96 well plate reader as previously reported.[10] The 100 μL reaction system contains 1 mM α -KG, 4 mM Asp, 1 mm NADH, 1 U/ml malate dehydrogenase and 0.1 mg/ml recombinant GOT1 protein, and then measures at absorbance of 340 nm. The degree of absorbance decrease was in direct proportion to GOT1 activity. Different concentrations of compounds were added to measure the inhibitory activity *in vitro*. Systat software SigmaPlot with PlotEnzyme Kinetics Module was used to analyze the enzyme activity.

Microscale Thermophoresis

Protein with AH binding capacity test was conducted according to the instructions using Monolith NTTM Protein Labeling Kit. GOT1 was labeled and diluted in 0.5 (v/v) % Tween-20 and 20 mM HEPES (pH 7.5), and then incubated with different concentration of AH 10 min at 37°C. Subsequently, the samples were load into capillaries and the thermophoresis was detected on a Monolith NT.115 (Nanotemper Technologies, Germany). Parameters setting were temperature 25°C, laser power 40% using 30 s on-time and LED power 100%. NTAnalysis software was used to calculate the K_d values.

Crystallography

Crystallization of GOT1 was performed using sitting-drop vapor diffusion method at 18°C for 48 h. Before crystalizing, protein samples (16 mg/mL) were mixed with AH at a final concentration of 40 μM and incubated on ice for 2 h, and then the precipitate was removed by centrifugation. Each drop included 0.25 μL protein, 0.25 μL precipitant

buffer (0.005 M Cobalt (II) chloride hexahydrate, 0.005 M Nickel (II) chloride hexahydrate, 0.005 M Cadmium chloride hydrate, 0.005 M Magnesium chloride hexahydrate, 0.1 M HEPES pH 7.5, 12% w/v Polyethylene glycol 3,350). Formed crystals were transferred in mother buffer supplemented with 25% [v/v] glycerol and flash-frozen in liquid nitrogen. Several attempts were made to obtain the lignan **5**, **7**, **13** bound structures using soaking and co-crystallization. Ultimately, we were not able to successfully achieve the co-crystallization data of these compounds and got1 protein.

GOT1 diffraction data were collected at Shanghai Synchrotron Radiation Facility (SSRF) in China. The data sets were processed using the HKL-2000 software.[22] The phasing was used molecular replacement (Phaser, CCP4) with the human GOT1 (PDB entry 6DND) to solve in a stepwise manner.[21,23] Subsequently, PHENIX and COOT software were used to manually refine the data and adjust structural models.[24,25] All figures were produced using PyMOL software.

Cell culture and viability assay

Pancreas (SW1990, AsPC-1, PANC-1), colorectal (HCT116), breast (HCC1806, MM231, MM453), ovarian cancer cell (ES2) and nonmalignant human pancreatic duct epithelial cell line (HDPE6C7) obtained from ATCC were cultured in 1640 media or Dulbecco's modified Eagle medium (DMEM) supplemented with 10% (v/v) fetal bovine serum (FBS), 100 μg/mL streptomycin and 100 U/ml penicillin. Cells were maintained in a humidified atmosphere of 5% CO_2 at 37°C.

MTT (3-(4,5-dimethylthiazol-2-yl)-2,5-diphenyl Tetrazoliumbromide) assay was

used to assess the cell viability. Briefly, cells were seeded in 96 well plates at a density of 5×10^3 cells per well for 24 h. Removed medium, and the cells were then treated AH at various concentrations (0.1-100 μM) with DMSO as a control. After incubation for 48 h, each well were added 100 μL MTT solution (2 mg/ml) and incubated at 37℃ for another 4 h. Dissolve the formed formazan crystals in DMSO (200 μL/well) and shake for 5 minutes. Then the absorbance of the solution was measured at 490 nm with amicroplate reader. The assay was carried out in triplicate.

Cell proliferation assay

Cells were seeded in 96-well plates (2×10^3 cells per well). To remove OAA, cells were inoculated in complete medium (2 mM Gln and 10 mM Glu) which was exchanged with culture media supplemented with 10% FBS the following day. The cells were fixed in 10% formalin and stained with 0.1% crystal violet. Extracted the dye with 10% acetic acid and determined the relative proliferation by OD at 595 nm.

Cell cycle assay

Propidium iodide (PI) staining was performed to determine the phase distribution of DNA content. Cells were treated with different concentrations of AH or vehicle for 48 h. After a series of treatment, the cell pellet was stained with 60 μg/mL RNase A and 30 μg/mL PI in the dark for 30 min. Finally, Flow cytometric analyses were performed by Cell-Quest software (Becton-Dickinson, USA). Cell cycle was measured by three independent experiments.

Cell apoptosis assay

The Annexin V-FITC apoptosis kit was purchased from USA BD Pharmingen™. In brief, different concentrations of AH was added into the wells for 48 h, and then harvested the cells. Resuspended them in annexin binding buffer and incubated with annexin V-FITC (10 mg/mL) and PI in the dark for 15 min. Flow cytometry was used to detect the stained cells and analyze the apoptosis immediately.

Wound healing assay

SW1990 cells were seeded into 6-well plates for 24h. Then a 10 μL pipette tip was used to make a straight scratch per well, after which the plates were washed with PBS to strip the floating cells and added AH (0-40 μM). Images from the same area of the wound were photographed under a microscope at 0-48 h.

Metabolomics analysis

SW1990 cell were grown to ~50% confluence in DMEM media with 10 mM glucose, 2 mM Gln and 5% FBS. Before two hours of metabolite collection, a complete media change was performed. Quantification Kits was used to determine the abundance of Gln (BioVision, #K55), malate (BioVision, #K637), OAA (Abcam, #ab83428) and Asp (Abcam, #ab102512). According the manufacturer's instruction, collected 20 mg cells and homogenized in 0.5 mL of provided buffers. After centrifuged, the supernatants were deproteinized with 10 K spin column, then compared and analyzed to standard curves.

Xenograft studies

Animal care and experiments were carried out in the Experimental Animal Center of Tongji Medical College, Huazhong University of Science and Technology, China. CB-17/scid mice (male, 8 weeks old) were purchased from commercial sources (Huafukang, China). SW1990-luc cells (3×10^6) resuspended using 0.1 ml PBS, were injected subcutaneously on the lower flank of mice. When tumors reached a diameter about 3 mm, the mice were randomly grouped into control model, 2.5 mg/kg and 5 mg/kg, and then injected intraperitoneal with AH or normal saline every day. Tumor size was measured using vernier caliper. After treatment for 2 weeks, the mice were sacrificed by deep anesthesia (Chloral hydrate, 10%, 10 μL/g) and then the metabolites of tumor tissues were detected according the method above. All animal experiments were carried out in accordance with the Guide for Care and Use of the Laboratory Animals of Huazhong University of Science and Technology, and approved by the Ethics Committee.

Statistical analysis

The collected data are expressed as mean ± SD. Graph-Pad-Prism 7.0 software was used to statistical analysis. One-way analysis of variance (ANOVA) used SPSS version 13.0 software to evaluate the multiple-group comparisons, and values of $p<0.05$ were considered statistically significant.

Results and Discussion

Detection of cyclobutyrolactone lignans against GOT1 activity

Based on the AO pharmacological activity, we identified the cyclobutyrolactone lignans from the in-house Natural Products Library against GOT1 activity. It can be divided into three groups according to the characteristics of the cores (**Fig S1**). Compound **6** (AH) exhibited similar inhibitory effect of GOT1 activity compared to AO in type II, **5** in type I and **13** in type III exhibited weaker inhibitory effect, while the activities of remaining lignans could not be detected (**Table 1**). Given the structural differences among these three types, type II has a hydroxyl-butyrolactone core, two isopentenyl side chains, as well as π-π stacking formed by the abundant double-strands, which may enhance the effects of the compound on GOT1 activity.

Although GOT1 metabolic target have been identified, few reports are currently available about GOT1 inhibitors. The inhibitory effect of AH (IC_{50} ~ 6.91 μM) is significantly stronger than the compound iGOT1-01 (IC_{50} ~ 85 μM) and its derivatives (**Fig 1C and S2**).[19,26] According to the design route and result of iGOT1-01, halogen, indole and other groups can be introduced to optimize the structure and activity of aspulvinone. The introduction of halogen into the compound scaffold is important, which can not only adjust the biological activity, but also serve as a reactive handle to achieve the diversification of intermediates.[27, 28] Microscale thermophoresis (MST) experiments further confirmed that the binding affinity between AH and GOT1 with a K_d was 8.53 ± 2.09 μM (**Fig 1D**). These findings suggested that aspulvinone with a hydroxyl-butyrolactone core can be used as a lead compound for the design and development of GOT1 inhibitors.

Co-crystal Structure of GOT1 and AH

We attempted co-crystallization of different compounds (**5**, **6**, **7**, **13**) with GOT1, and only the complex structure of GOT1-AH was obtained. Crystallization of GOT1 in the presence of AH afforded the opportunity to gain more detailed insight into the binding mode of compound AH within the GOT1 active site. The resolution of the complex structure was solved to 2.6 Å (PDB ID 6LIG). The statistics of data collection and refinement were listed in **Table 2**. The overall structure contains one large (residues 68-300) and two small (residues 17-67, 301-411) domains, with a core architecture consisting of an extended mixed α-helices and β-sheet through the active cavity of the protease and has been previously described in detail (**Fig 2A**).[21,29] The large regions in the dimer are fundamentally identical, while two active sites show different substrate accessibility.[30] Crystals soaked with the inhibitor AH showed that chain A bound AH at the cleft in the interface of the subunits, whereas in chain B a PLP was situated (**Fig 2B and 2C, Fig S3A**). As expected, AH adopts a compact conformation in the bulk solvent of GOT1, which fully occupies the active site. The surface electrostatic potential indicates that the active site pockets is electropositivity with some hydrophilic patches for substrate recognition (**Fig S3B**). Structural comparison using PDBeFold and DALI servers revealed that there are few changes between chain A of GOT1-AH and wild-type GOT1 (PDB ID 6DND), with a Z-score of 24.1 and root-mean-square deviation (RMSDs) of 0.32 Å over 410 residues. Overlapping these two structures, it was found that they can well coincide and the main active sites are similar, in which AH was occupied the PLP sites (**Fig S3C and S3D**). The hydroxyl-butyrolactone core

of AH is located in the same position as the phenolic oxygen of PLP, forming a rich interaction with surrounding amino acids. Moreover, the main difference is that Tyr71 and Ser297 in the opposite monomer constitute the active cavity of AH, which may play a function in stabilizing AH.

Detailed analysis showed that AH is stacked in residues Gly39, Thr110, Trp141, Asp223, Tyr226 and Phe361 by hydrophobic interactions, while the isopentenyl group in AH at the entrance is interacting with Ser297 and Tyr71 from the other subunit (**Fig 3A**). In addition, the side chains of Gly109, Ser258, Arg267 and Asn195 are hydrogen bonded to O4, O32 and O26 of AH, respectively (**Fig 3B**). Interestingly, the CE atom of AH is covalently linked to the NZ atom of Lys259 in a large domain through an isopentyl-linkage, similar to the PLP in chain A of wild-type enzyme which the N2A atom links to an internal Schiff base.[30] According to the chemical structure of AH, it may form a strong π-π stacking effect with GOT1. In chain B, the residual electron density clearly reveals the presence of PLP that forms hydrogen bonds with Thr110, Tyr226, Ser258 and Arg267 (**Fig S4**). The rich hydrogen bonding network in the active site contributes to stabilize spatial structure of proteins and perform their physiological functions.[31] When the hydrogen bonding network formed by PLP is disturbed, the co-factors cannot be activated, resulting in the reduction or ablation of GOT1 activity.

From the SAR analysis, the presence of the two isopentenyl side chains greatly enhances the lipophilicity of the compound, making it easier for the compound to pass through the lipid soluble cell membrane and combine with the target protein, improving the biological activity and bioavailability of the compound.[32] Concomitantly, its unique

π-π conjugation enhances the stability of the compound, facilitates the electron transfer, and improves the affinity selectivity of the compounds.

AH inhibited activity in cancer cells

To explore the anti-tumor activity of AH, several human cancer cell lines including pancreas (AsPC-1, PANC-1, SW1990), breast (HCC1806, MM231, MM453), colorectal (HCT116), ovarian cancer cell (ES2), along with nonmalignant human pancreatic duct epithelial cell line (HDPE6C7) were selected to detect the inhibitory effect of AH on their growth. After treatment for 48 h, AH exhibited significant cytotoxicity effects on SW1990, PANC-1, AsPC-1 cell lines compared to the other cell lines with IC_{50} ranging from 6.32 to 10.47 μM (**Fig 4**). Importantly, AH exhibited minimal cytotoxicity effects on the normal cell lines HPDE6C7 with IC_{50} value over 100 μM. These data exhibited that AH possess selectivity cytotoxicity and anti-proliferation against PDAC cells.

AH modulates metabolism and ROS response

GOT1 is participated in the production of Gln-dependent NADPH in PDAC and catalyzes the reversible conversion of Asp to OAA. To investigate the AH effects on Gln metabolism, the associated metabolites including OAA, malate (Mal) were detected. As shown in **Fig 5A**, AH treatment reduced the content of OAA and Mal, while accumulated Asp correspondingly. Consequently, the ratio of $NADPH/NADP^+$ was remarkably decreased (**Fig 5B**). As excessive reactive oxygen species (ROS) could

enhance cellular oxidative stress, resulting in damage to DNA, proteins or lipids, causing apoptosis or necrosis,[33] we examined the physiological correlation between AH treatment and ROS response. 2,7-Dichlorofluorescein diacetate (DCFDA) was used to measure the intracellular ROS levels. In SW1990 cells, ROS is positively relevance with AH concentration, indicating that cells inhibit the activity of GOT1 by up-regulating ROS levels (**Fig 5C and 5D**). The above data indicated that AH treatment could block the production of Gln-dependent NADPH and participate in the redox homeostasis of PDAC cells.

AH treatment affected the apoptosis, cell cycle, proliferation and migration in SW1990 cells

In addition to inhibiting cell proliferation, we also investigated the mechanism of growth inhibition induced by AH with flow cytometry. The double staining of FITC-Annexin V and propidium iodide (PI) revealed that AH could dose-dependently induce apoptosis in SW1990 cells. After 48 h incubation at the concentration of 10 μM, 20 μM and 40 μM, the induction rates were 4.6%, 9.5% and 28.3%, 80.2%, respectively (**Fig 6A**). Simultaneously, treated cells in the same way to survey the cell cycle distributions. Analysis results from flow cytometry indicated that AH mainly induced S phase arrest of SW1990 cells. In detail, AH could increase the proportion of S phase cells (25.1%, 32.5%, 38.6%, 43.9%) with a tiny decrease in the G0/G1 phase (68.2%, 59.4%, 48.6%, 43.5%) (**Fig 6B**). Subsequently, the EDU staining analysis and wound healing cell migration test also proved the anti-proliferation effect of AH in SW1990 cells (**Fig 6C-**

E), with a dose and time dependent manner. These results suggested that AH treatment could prevent the cell cycle in G1/S transition, resulting in a decrease rate of cell growth and cycle progression in PDAC cells.

In vivo antitumor activity of AH

Next, the anti-tumor effect of AH *in vivo* was evaluated in the CB-17/scid mice xenograft model. One week after subcutaneous injection of PDAC cells into the lower flank of mice, intraperitoneal injection of vehicle or AH (2.5 mg/kg/d and 5 mg/kg/d) treated to mice for 14 days. As presented in **Fig 7 A-D**, the tumor volume of the experimental group was significantly smaller than that of the control group, suggesting that AH had inhibitory effect on the growth of SW1990 xenografts. Detection of tumor tissue metabolites found that OAA and Mal decreased while Asp and Gln accumulated correspondingly. Therefore, the proportion of NADPH/$NADP^+$ was accompanied by a decrease, consistent with the effect *in vitro* (**Fig 7E and 7F**). Moreover, there was no significant change in the body weight and histomorphology of the mice, indicating that AH was an effective and safe anti-tumor agent.

Conclusions

Analysis the structure of cyclobutyrolactone lignans showed that aspulvinone with hydroxyl-butyrolactone core and unique conjugated structure may result in different enzyme activities. Moreover, the double isopentenyl structure may also enhance the function of aspulvinone. Further, the complex crystal structure of AH and GOT1

intuitively illustrates its binding mode, that is, AH located at the interface of the large and small domain competes with PLP for active sites. Two oxygen atoms of the hydroxyl-butyrolactone core form four hydrogen bonds to the backbone of Gly109, Ser258 and Arg267. Unlike the rich hydrogen bonding network formed by PLP, AH breaks this stable binding, thereby destroying the activity of the enzyme. These results support the finding that AH operates through direct competition for the active site.

In addition, we demonstrated that AH has selective cytotoxic on pancreatic cancer cells and inhibits the proliferation of SW1990 cells. Further, we confirmed that it blocks the cell cycle in the G1/S transition, induces cell apoptosis, and inhibits the xenograft model induced by SW1990 cells. The relevant metabolites *in vivo* and *in vitro* were detected, exhibiting that the $NADPH/NADP^+$ ratio and ROS content were increased. All of these indicate that AH has a suppressive effect on PDAC growth.

The current study provides insight into the binding mode of protease inhibitors and offers new strategies for further drug development. More potent and safer GOT1 inhibitors are expected to become available for clinical applications.

Acknowledgments

We thank the staff from BL17U1/BL19U1 beamline of National Center for Protein Sciences Shanghai (NCPSS) at Shanghai Synchrotron Radiation Facility, for assistance during data collection. This work is supported by the National Natural Science Foundation of China (No. 81703580), the National Natural Science Foundation of China (No. 82003633), and the Program for Changjiang Scholars of Ministry of

Education of the People's Republic of China (No. T2016088).

Conflict of interest

The authors declare no competing interest.

Data availability statement

The complex structure of AH and GOT1 was deposited in PDB (http://www.wwpdb.org/) with the accession code 6LIG. All other data are included in the main article and supplementary materials.

Abbreviations

GOT1, glutamic oxaloacetate transaminase 1; PDAC, Pancreatic ductal adenocarcinoma; AH, Aspulvinone H; PLP, pyrido-aldehyde 5-phosphate; SAR, structure-activity relationship; OAA, oxaloacetate; MDH1, malate dehydrogenase 1; ME1, malic enzyme 1; NPs, natural products; SBDD, structure-based drug design; AO, Aspulvinone O; MST, microscale thermophoresis; RMSD, root-mean-square deviation; ROS, reactive oxygen species.

References

1. Haeberle L, Esposito I. Pathology of pancreatic cancer. Transl Gastroenterol Hepatol 2019;4:50-50.
2. Grønningsæter IS, Reikvam H, Aasebø E, Brevik SB, Tvedt TH, Bruserud Ø,

Hatfield KJ. Targeting Cellular Metabolism in Acute Myeloid Leukemia and The Role of Patient Heterogeneity. Cell 2020;9:1155.

3. Heiden MGV, Cantley LC, Thompson CB. Understanding the Warburg Effect: The Metabolic Requirements of Cell Proliferation. Science 2009;324:1029-1033.
4. Son JY, Lyssiotis CA, Hao QY, Wang XX, Hua SJ, Ligorio M, Perera RM, Ferrone CR, Mullarky E, Chang NS, Kang YA, Fleming JB, Bardeesy N, Asara JM, Haigis MC, DePinho RA, Cantley LC, Kimmelman AC. Glutamine supports pancreatic cancer growth through a KRAS-regulated metabolic pathway. Nature 2013;496:101-105.
5. Li DD, Fu ZQ, Chen RW, Zhao XH, Zhou Y, Zeng BM, Yu M, Zhou QB, Lin Q, Gao WC, Ye HL, Zhou JJ, Li ZH, Liu YM, Chen RF. Inhibition of glutamine metabolism counteracts pancreatic cancer stem cell features and sensitizes cells to radiotherapy. Oncotarget 2015;6:31151-31163.
6. Chakrabarti G, Boothman DA. Abstract 1679: Inhibiting KRAS-reprogrammed glutamine metabolism sensitizes pancreatic cancer to NQO1-bioactivatable drugs. Cancer Research 2014;74:1679-1679.
7. Lyssiotis CA, Son J, Cantley LC, Cantley LC, Kimmelman AC. Pancreatic cancers rely on a novel glutamine metabolism pathway to maintain redox balance. Cell cycle 2013;12:1987-1988.
8. Halbrook CJ, Lyssiotis CA. Employing Metabolism to Improve the Diagnosis and Treatment of Pancreatic Cancer. Cancer Cell 2017;31:5-19.
9. Weinberg F, Hamanaka R, Wheaton WW, Weinberg S, Joseph J, Lopez M,

Kalyanaraman B, Mutlu GM, Budinger GR, Chandel NS. Mitochondrial metabolism and ROS generation are essential for Kras-mediated tumorigenicity. Proc Natl Acad Sci USA 2010;107:8788-8793.

10. Sun WG, Luan SS, Qi CX, Yan S, Li H, Zhang YH. Aspulvinone O, a natural inhibitor of GOT1 suppresses pancreatic ductal adenocarcinoma cells growth by interfering glutamine metabolism. Cell Communication & Signaling 2019;17:111.
11. Abrego J, Gunda V, Vernucci E, Shukla SK, King RJ, Dasgupta GoodeA, Murthy D, Yu F, Singh PK. GOT1-mediated anaplerotic glutamine metabolism regulates chronic acidosis stress in pancreatic cancer cells. Cancer Lett 2017;400:37-46.
12. Wise DR, Thompson CB. Glutamine addiction: a new therapeutic target in cancer. Trends in biochemical sciences 2010;35:427-433.
13. Márquez J, Alonso FJ, Matés JM, Segura JA, Rufián M, Campos-Sandoval J. Glutamine addiction in gliomas. Neurochemical Research 2017;42:1735-1746.
14. Newman DJ, Cragg GM. Natural Products as Sources of New Drugs over the Nearly Four Decades from 01/1981 to 09/2019. Journal of Natural Products 2020;83:770-803.
15. Bauer A. Story of Eribulin Mesylate: Development of the Longest Drug Synthesis. Top Heterocycl Chem 2016;44:209-270.
16. Patridge E, Gareiss P, Kinch MS, Hoyer D. An analysis of FDA-approved drugs: natural products and their derivatives. Drug Discovery Today 2016;21:204-207.
17. Leonardo F, Ricardo DS, Glaucius O, Andricopulo AD. Molecular Docking and Structure-Based Drug Design Strategies. Molecules 2015;20:13384-13421.

18. Congreve M, Andrews S. Perspective in Medicinal Chemistry: Structure-Based Drug Design. Current Topics in Medicinal Chemistry 2016;17:93-94.
19. Holt MC, Assar Z, Zavareh RB, Lin L, Anglin J, Mashadova O, Haldar D, Mullarky E, Kremer DM, Cantley LC, Kimmelman AC, Stein AJ, Lairson LL, Lyssiotis CA. Biochemical characterization and structure-based mutational analysis provides insight into binding and mechanism of action of novel aspartate aminotransferase inhibitors. Biochemistry 2018;57:6604-6614.
20. Śledź P, Caflisch A. Protein structure-based drug design: from docking to molecular dynamics. Current Opinion in Structural Biology 2017;48:93-102.
21. Cruz PG, Auld DS, Schultz PJ, Lovell S, Battaile KP, MacArthur R, Shen M, Castillo GT, Inglese J, Sherman DH. Titration-Based Screening for Evaluation of Natural Product Extracts: Identification of an Aspulvinone Family of Luciferase Inhibitors. Chemistry & Biology 2011;18:1442-52.
22. Terwilliger TC. Automated structure solution, density modification and model building. Acta Crystallographica 2002;58:1937-1940.
23. Mccoy AJ, Grossekunstleve RW, Adams PD, Winn MD, Storoni LC, Read RJ. Phaser crystallographic software. Journal of applied crystallography 2007;40:658.
24. Adams PD, Afonine PV, Bunkóczi G, Chen VB, Davis IW, Echols N, Headd JJ, Hung LW, Kapral GJ, Kunstleve RWG, McCoy AJ, Moriarty NW, Oeffner R, Read RJ, Richardson DC, Richardson JS, Terwilliger TC, Zwart PH. PHENIX: a comprehensive Python-based system for macromolecular structure solution. Acta Crystallographica 2010;66:13.

25. Emsley P, Cowtan K. Coot: model-building tools for molecular graphics. Acta Crystallographica 2004;60:2126-2132.
26. Anglin J, Zavareh RB, Sander PN, Haldar D, Mullarky E, Cantley LC, Kimmelman AC, Lyssiotis CA, Lairson L. Discovery and optimization of aspartate aminotransferase 1 inhibitors to target redox balance in pancreatic ductal adenocarcinoma. Bioorganic & Medicinal Chemistry Letters 2018;28:2675-2678.
27. Latham J, Brandenburger E, Shepherd SA, Menon BRK, Micklefield J. Development of Halogenase Enzymes for Use in Synthesis. Chemical Reviews 2018;118:232-269.
28. Lu YX, Liu YT, Xu ZJ, Li HY, Liu H, Zhu W. Halogen Bonding for Rational Drug Design and New Drug Discovery. Expert Opin Drug Discovery 2012;7:375−383.
29. Rhee S, Silva MM, Hyde CC, Rogers PH, Metzler CM, Metzler DE, Arnone A. Refinement and Comparisons of the Crystal Structures of Pig Cytosolic Aspartate Aminotransferase and Its Complex with 2-Methylaspartate. Journal of Biological Chemistry 1997;272:17293-17302.
30. Dajnowicz S, Parks JM, Hu XC, Gesler K, Kovalevsky AY, Mueser TC. Direct evidence that an extended hydrogen-bonding network influences activation of pyridoxal 5-phosphate in aspartate aminotransferase. Journal of Biological Chemistry 2017;292:5970-5980.
31. Dajnowicz S, Johnston RC, Parks JM, Blakeley MP, Keen DA, Weiss KL, Gerlits, O, Kovalevsky A, Mueser TC. Direct visualization of critical hydrogen atoms in a pyridoxal 5′-phosphate enzyme. Nature Communications 2017;8:955.

32. Bifulco M, Malfitano AM, Proto MC, Santoro A, Caruso M, Laezza C. Biological and Pharmacological Roles of N6-Isopentenyladenosine: An Emerging Anticancer Drug. Anti-Cancer Agents in Medicinal Chemistry 2008;8:200-204.
33. Zhou B, Zhang JY, Liu XS, Chen HZ, Ai YL, Cheng K, Sun RY, Zhou DW, Han JH, Wu Q. Tom20 senses iron-activated ROS signaling to promote melanoma cell pyroptosis. Cell Research 2018;28:1171-1185.

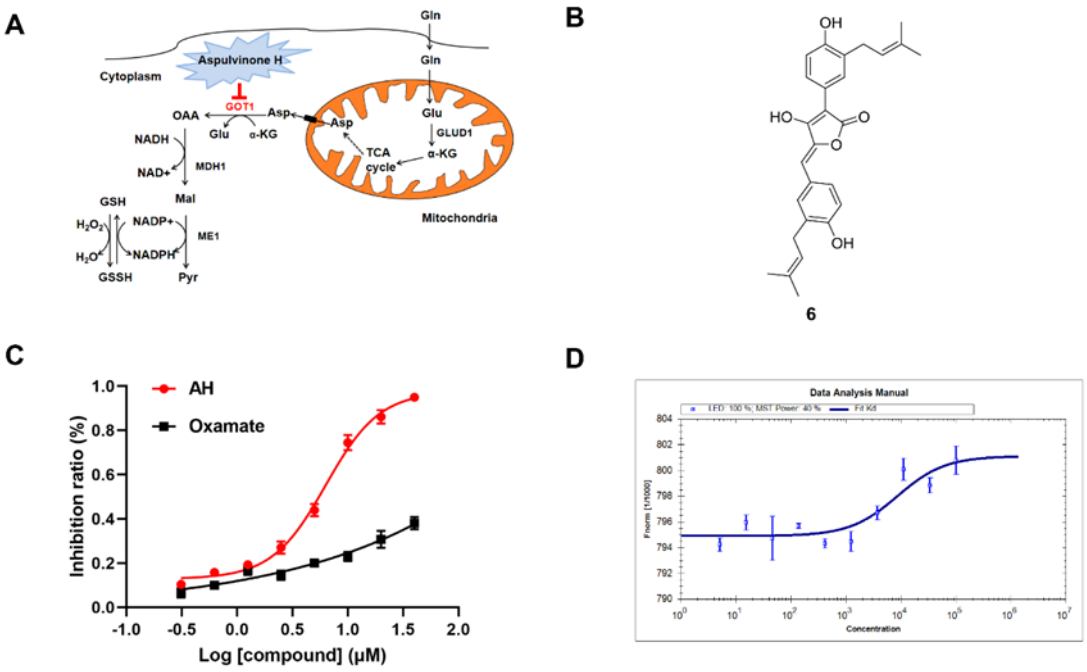

Fig 1. AH selectively targets GOT1. (A) Schematic overview of GOT1-mediated Gln metabolism. (B) The chemical structures of AH. (C) AH selectively inhibited GOT1 activity. (D)MST assay of the K_d value between AH and GOT1.

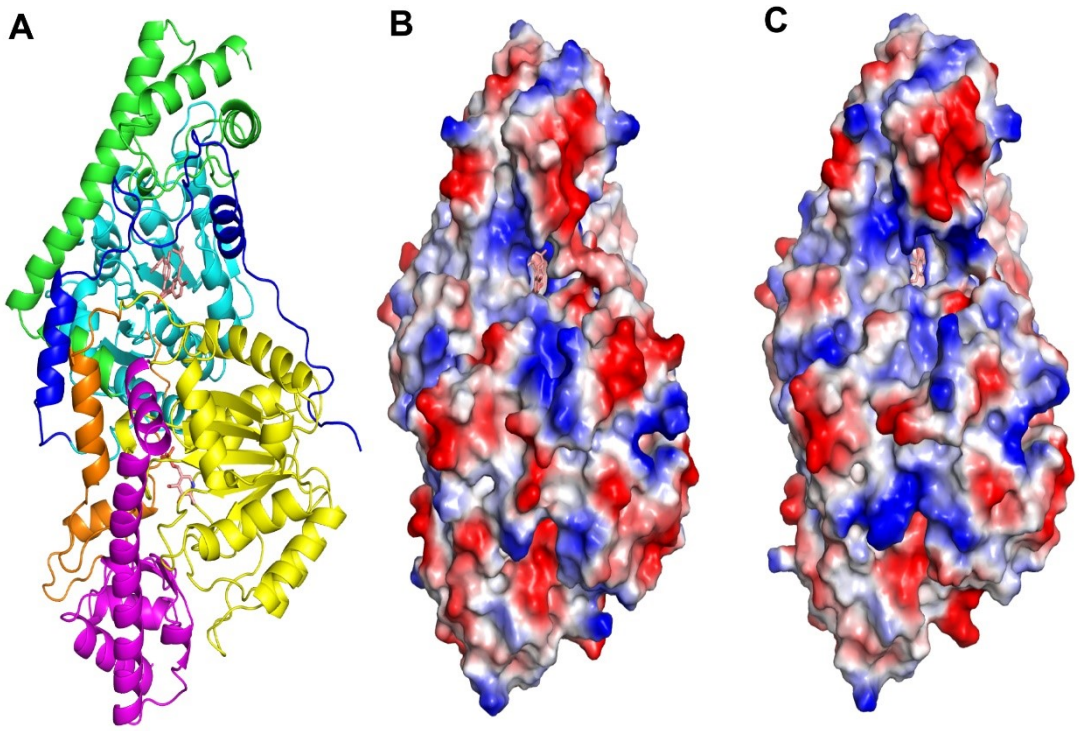

Fig 2. Structural of GOT1 in complex with AH. (A) Overall structure of GOT1-AH. the small domain 1 (blue/orange) includes two short α helix structures, domain 2 (cyan/yellow) is a smaller $(\alpha/\beta)_7$ sandwich fold, domain 3 (green/magenta) close to domain 1. Surface representation of AH (B) and PLP (C) into the active site of GOT1. electrostatic potential show that the active site pocket is positively charged. Blue, positive potential; red, negative potential; white, neutral potential.

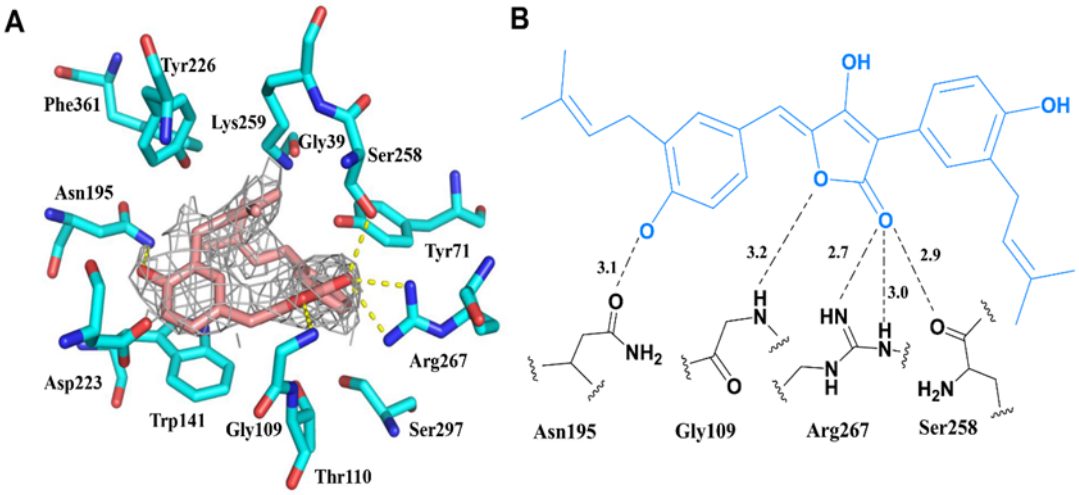

Fig 3. Detailed view of the active site. The *2Fo-Fc* electron density of AH bound to chain A (A) is shown as a gray mesh. The map is contoured at the 1σ level. Side chains involved in binding site are shown. (B) Schematic of the potential hydrogen bonding network between AH (blue)and GOT1(black).

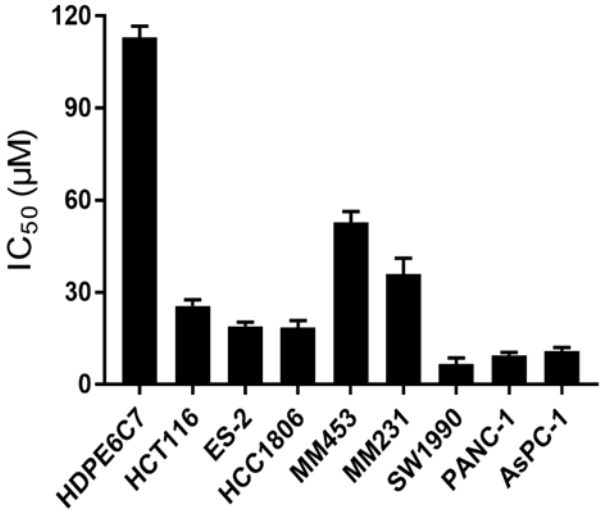

Fig 4. The IC_{50} values of AH for indicated cell lines. Cells were treated with AH at various concentrations (0.1-100 μM) for 48 h and determined using the MTT assay.

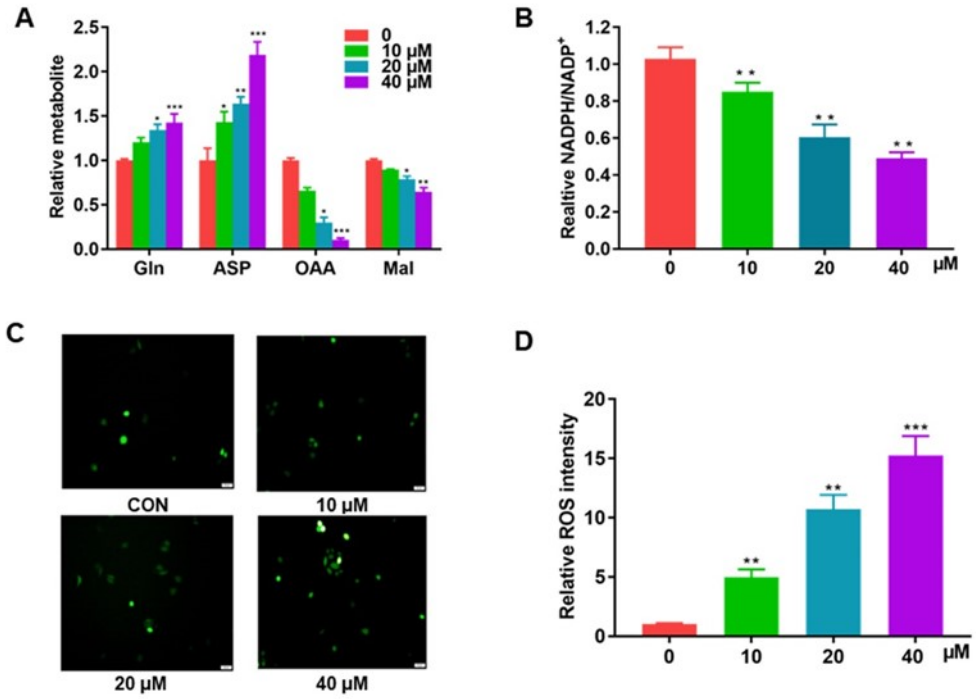

Fig 5. AH treatment induced Gln metabolism and maintained redox balance. (A) The effect of AH treatment (10, 20, 40 μM) on relative metabolite abundance in SW1990 cells. (B) The effect of AH treatment (10, 20, 40 μM) on $NADP^+$/NADPH ratio in SW1990 cells. (C, D) Intracellular ROS level measurement using carboxyH2DCFDA with 10, 20, 40 μM AH. Data represent means ± SD of three experiments. *P < 0.05, **P < 0.01, ***P < 0.001 compared with the control group.

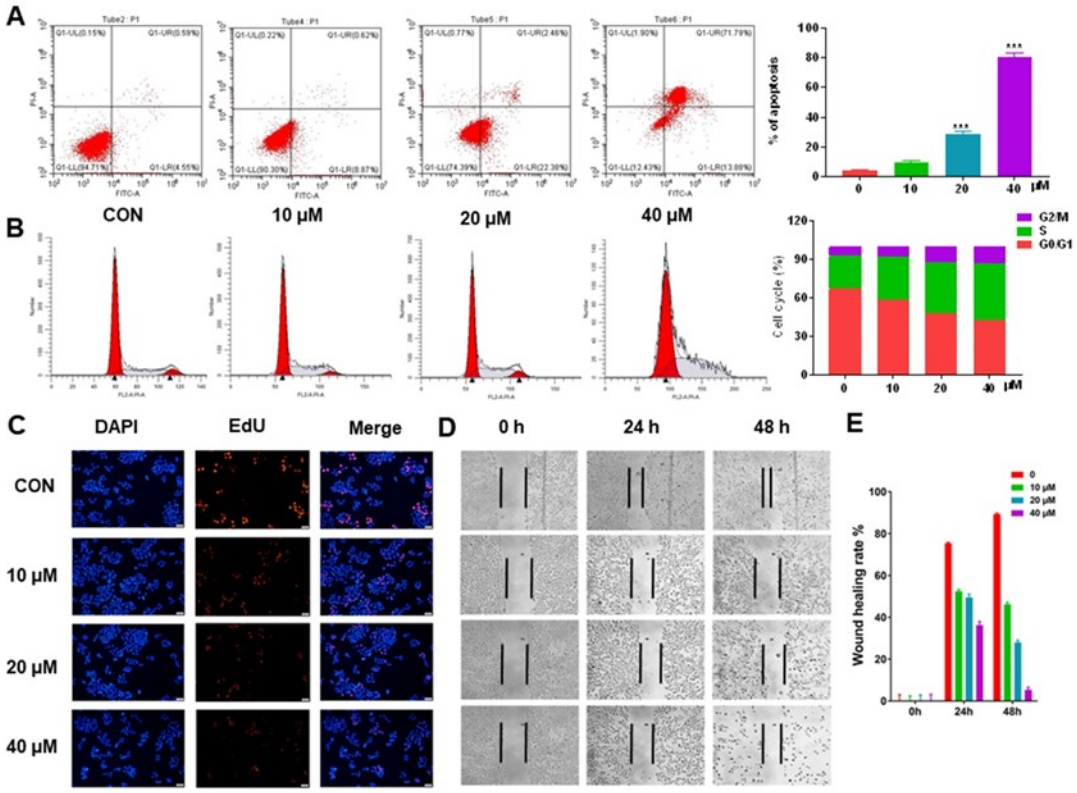

Fig 6. AH treatment affected the apoptosis, cell cycle and proliferation in SW1990 cells. (A) Evaluated and quantified analysis of SW1990 cells apoptosis using PI/AnnexinV-FITC double staining after treatment with AH for 24 h. (B) Cell cycle distribution analysis of SW1990 cells induced by AH. (C) DAPI and EDU double staining was used to assay the effect of AH on the proliferation of SW1990 cells. (D) Wound healing assay in SW1990 cells with indicated treatments at 0 h, 24 h and 48 h. (E) Quantitative analysis of wound healing assay. Data represent means ± SD of three experiments. *P < 0.05, **P < 0.01, ***P < 0.001 compared with the control group.

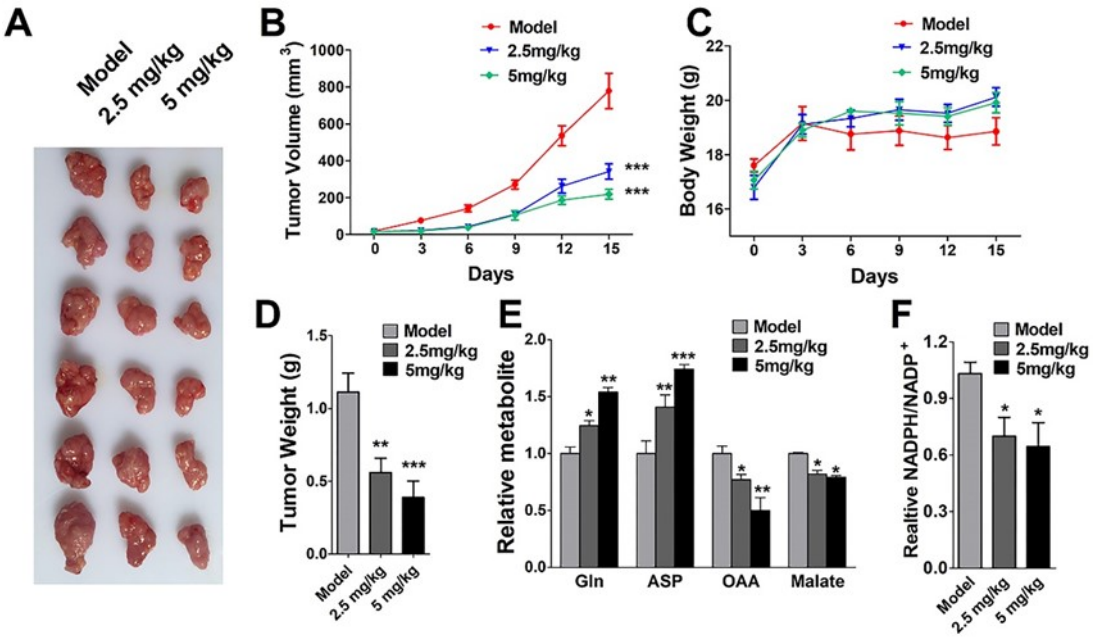

Fig 7. Evaluation of the *in vivo* efficacy of AH in xenograft tumors. (A) tumor sample of xenograft mice after 14 days treatment. Tumor volume (B), body weight (C) and tumor weight (D) for SW1990 xenografts in CB-17/scid mice treated with 2.5 or 5 mg/kg/day AH for 14 consecutive days. (E) Effect of metabolite abundance in different groups of tumor tissues. (F) NADPH/$NADP^+$ ratio in different groups of tumor tissues. Variance (ANOVA) was used to compare the differences among groups. Data represent mean ± SD. *P < 0.05, **P < 0.01, ***P < 0.001 compared with the control group.

Table 1. GOT1 inhibition activity of lignans

Compounds		IC_{50}† (μM)	Compounds		IC_{50} (μM)
1	Terrusnolide B	> 40	**11**	Asperlide A	> 40
2	Terrusnolide D	> 40	**12**	Asperlide B	> 40
3	Terrusnolide C	> 40	**13**	(+)-3',3'-di-(dimethylallyl)-butyrolactone II	26.38 ± 0.12
4	(+)-asperteretone C	> 40	**14**	Isobutyrolactone V	> 40
5	(+)-asperteretone B	19.16 ± 0.15	**15**	Butyrolactone V	> 40
6	Aspulvinone H	6.91 ± 0.04	**16**	Butyrolactone VI	> 40
7	Aspulvinone O	6.02 ± 0.03	**17**	Butyrolactone IV	> 40
8	Butyrolactone III	> 40	**18**	Butyrolactone I	> 40
9	Versicolactone B	> 40	**19**	Aspernolide E	> 40
10	Butyrolactone II	> 40			

† IC_{50} = 50% inhibitory concentration (means ± SD of 3 independent experiments).

Table 2. Data collection and refinement statistics.

parameter	Enzyme in complex with AH
Resolution (Å)	49.58–2.62 (2.714–2.62)
Space group	P 1 2_1 1
Unit cell dimensions	a=64.87 Å, b=90.42 Å, c=74.05 Å;
	α=90.0°, β =91.87°, γ=90.0°
Unique reflections	25267 (2557)
Multiplicity	2.0 (2.0)
Completeness (%)	97.67 (97.93)
$I/\sigma(I)$	9.34 (2.99)
R-merge† (%)	0.07031 (0.2735)
R-work	0.2127 (0.2690)
R-free	0.2661 (0.3291)
Number of non-hydrogen atoms	6,703
Protein residues	820
r.m.s.d.from ideal geometry	
Bonds lengths (Å)	0.002
Angles (°)	0.46
Ramachandran plot (%)	
Favored	96.94
Outliers	0.12
Clashscore	4.51
Average *B*-factor	29.95
PDB code	6LIG

†*R*-merge = $\Sigma_{hkl}\ \Sigma_i\ |I_i(hkl)-<I(hkl)>|/\Sigma_{hkl}\ \Sigma_i\ I_i(hkl)$, where $I(hkl)$ is the intensity of reflection *hkl*, Σ_{hkl} is the sum over all reflections and Σ_i is the sum over *i* measurements of reflection *hkl*. Statistics for the highest-resolution shell are shown in parentheses.